Mineralogical Magazine, February 2018, Vol. 82(1), pp. 23–33

Transmission electron microscopy study of the epitaxial association of hedenbergite whiskers with babingtonite

MARIKO NAGASHIMA[1,*] AND DAISUKE NISHIO-HAMANE[2]

[1] Graduate School of Sciences and Technology for Innovation, Yamaguchi University, Yamaguchi 753-8512, Japan
[2] The Institute for Solid State Physics, the University of Tokyo, Kashiwa, Chiba 277-8581, Japan

[*Received 9 November 2016; Accepted 16 March 2017; Associate Editor: Anthony Kampf*]

ABSTRACT

Overgrowths of whiskers of hedenbergite ($Ca(Fe^{2+},Mg)Si_2O_6$) on the hydrous pyroxenoid babingtonite ($Ca_2Fe^{2+}Fe^{3+}[Si_5O_{14}(OH)]$) have been observed at Arvigo in Switzerland and Kreimbach/Kaulbach in Germany, and we have studied them with transmission electron microscopy in order to understand their structural relationships and formation. The boundaries between babingtonite and hedenbergite are sharply defined, and the two minerals are in direct contact with no additional phases present. The relationships of babingtonite (Bab) and hedenbergite (Hd) were determined as Bab[100]//Hd[112] in the Arvigo specimen and Bab[$\bar{1}$00]//Hd[1$\bar{1}$2] in the Kreimbach/Kaulbach specimen. Diffraction derived from Bab(031) and Hd (02$\bar{1}$) in the Arvigo samples and Bab(031) and Hd(021) in the Kreimbach/Kaulbach samples were observed in identical positions. The reciprocity between the babingtonite and hedenbergite structures is governed by the direction of the SiO_4-tetrahedral chains, and the related configuration of octahedra. Thus, hedenbergite is apparently an epitaxial phase grown on a base of {010} plates of babingtonite. The defined orientation relationship is also consistent with that shown in topotaxial intergrowths of other clinopyroxenes and pyroxenoids. The topotaxial intergrowths may result from diffusion-controlled solid-state reactions, whereas rapid whisker growth is characteristic of supersaturated solutions or a vapour medium. The epitaxial growth of hedenbergite whiskers on babingtonite with an abrupt but coherent change of structure at the interface represents an ideal example where the similar chemical compositions of host and guest contribute strongly to the close structural relationship.

KEYWORDS: babingtonite, clinopyroxene, epitaxy, intergrowth, transmission electron microscopy.

Introduction

BABINGTONITE, $Ca_2Fe^{2+}Fe^{3+}[Si_5O_{14}(OH)]$ ($Z = 2$, space group $P\bar{1}$), is a hydrous pyroxenoid-group mineral with undulating chains of five-periodic SiO_4 tetrahedra (*fünfer* single chains of Liebau, 1985). In addition, the crystal structure of babingtonite (Araki and Zoltai, 1972) has two 8-coordinated Ca sites and two crystallographically non-equivalent octahedrally coordinated sites, M1 (Fe^{2+}) and M2 (Fe^{3+}). The ranges of babingtonite unit-cell parameters are $a = 7.466$–7.478 Å, $b = 11.623$–11.642 Å, $c = 6.681$–6.690 Å, $\alpha = 91.53$–$91.59°$, $\beta = 93.86$–$93.94°$, $\gamma = 104.20$–$104.34°$ and $V = 560.2$–562.3 Å^3 (Nagashima *et al.*, 2014). Babingtonite typically occurs in hydrothermally altered zeolite-dominant veins and cavities in basic igneous rocks (e.g. Burt, 1971; Birch, 1983; Wise and Moller, 1990; Akasaka *et al.*, 2013), and in skarn deposits (e.g. Gole, 1981; Burns and Dyar, 1991).

Clinopyroxenes with diopside ($CaMgSi_2O_6$) and hedenbergite ($CaFe^{2+}Si_2O_6$) components also occur in skarns. The crystal structure of the clinopyroxene is characterized by two-periodic chains of corner-sharing SiO_4 tetrahedra running along the *c* axis. The chains are linked laterally by Ca in 8-coordinated polyhedra, and Mg and Fe^{2+} ions centring octahedra (e.g. Cameron *et al.*, 1973). The unit-cell parameters vary due to Mg ↔ Fe^{2+}

*E-mail: nagashim@yamaguchi-u.ac.jp
https://doi.org/10.1180/minmag.2017.081.020

substitution (e.g. Nolan, 1969; Rutstein and Yund, 1969) as follows: $a = 9.75–9.87$ Å, $b = 8.92–9.03$ Å, $c = 5.23–5.25$ Å, $\beta = 104.4–105.8°$ and V = 439.0–451.2 Å^3 ($Z = 4$, space group $C2/c$). Although Di–Hd series clinopyroxenes rarely coexist with babingtonite, several authors have reported epitaxial whiskers of these clinopyroxenes on babingtonite, as for example, in a quarry at Kreimbach/Kaulbach, Kaiserslautern, Germany (Heidtke, 1986; Bungert *et al*., 1992), at Arvigo, Grisons, Switzerland (Armbruster *et al*., 2000) and at Lincoln Park near Paterson, New Jersey, USA (Armbruster *et al*., 2002). On the basis of the morphological and crystal structural features of babingtonite and hedenbergite, Armbruster *et al*. (2000, 2002) demonstrated that hedenbergite [001] whiskers emerge out of the babingtonite (010) face. Thus, the five-periodic silicate chains in babingtonite continue as two-periodic chains in hedenbergite.

In this study, we report on our investigation into the epitaxial association of platy babingtonite overgrown by clinopyroxene whiskers from two different localities: (1) Arvigo, Grisons, Switzerland (NMBE34974); and (2) Kreimbach/Kaulbach, Kaiserslautern, Germany. We used transmission electron microscopy (TEM) to determine the orientation and to provide structural information on the interfaces between both phases.

Sample descriptions

Sample NMBE34974 (Fig. 1*a*–*c*) was collected at Arvigo, Val Calanca, Grisons, Switzerland, where alpine fissures and fractures contain the epitaxial assemblage of hedenbergite fibres on babingtonite associated with epidote, titanite, prehnite, adularia (a variety of K-feldspar), chlorite and calcite (Graeser and Stadler, 1976). The country rock is banded biotite gneiss intercalated with a light-coloured two-mica gneiss and rare calc-silicate lenses (Armbruster *et al*., 2000). The assemblage of fissure minerals varies as an indicator of the conditions of formation, and the assemblage indicates a decrease in grade from the prehnite–pumpellyite facies to the zeolite facies (Weisenberger and Bucher, 2010, 2011). The influence of variations or fluctuations in f_{O_2} and water activity on the formation of epitaxial hedenbergite on babingtonite was discussed by Armbruster *et al*. (2002). Our sample (NMBE34974) studied here consists of a few intergrown heulandite crystals covered by chlorite. A green central crystal of babingtonite (~0.15 mm in size) with a dense felt of white fibres was investigated in detail.

Another sample (Fig. 1*d* and *e*) was collected from the Kreimbach/Kaulbach quarry, ~15 km NW of Kaiserslautern, Germany, where babingtonite associated with epitaxial fibres occurs in fissures in hydrothermally altered diorite, along with various secondary minerals. The following two assemblages of fissure minerals were identified by Heidtke (1986): (1) calcite I + pumpellyite I + chlorite + pumpellyite II + prehnite + opaque minerals + pectolite + albite + calcite II + apophyllite + analcime; and (2) quartz + datolite + pumpellyite + julgoldite + hematite + lepidocrocite, and it was in the interstices of aggregates of calcite II that black to greyish-green platy crystals with overgrowths of white epitaxial fibres were reported. The platy crystals were later identified as babingtonite (Bungert *et al*., 1992), but the white fibres covering the plates were misidentified as pectolite. Although fibrous pectolite crystals are also sometimes associated with babingtonite, they do not occur as epitaxial fibres on babingtonite plates. By applying single-crystal X-ray diffraction methods, Armbruster *et al*. (2002) concluded that the fibres on the babingtonite at this locality are hedenbergite. The hydrothermal minerals in the Kreimbach/Kaulbach area (prehnite, pectolite, datolite, apophyllite and julgoldite) formed after cooling to the *P*–*T* conditions of the prehnite–pumpellyite facies (Hofmeister and von Platen, 1990).

At both localities, white ferroan diopside or magnesian hedenbergite fibres (hereafter simply called hedenbergite) are inclined at angles of 100°–105° relative to the platy basis of the deep-green babingtonite (e.g. Fig. 1*b*). The epitaxial hedenbergite whiskers in the Arvigo sample (Fig. 1*a*–*c*) tend to be longer than those in the Kreimbach/Kaulbach sample. In the Arvigo specimen, fibres of hedenbergite also occur in complex arrays between platy-shaped grains of babingtonite (Fig. 1*c*).

Experimental

Scanning electron microscope observations

Scanning electron images of the Arvigo specimen (Fig. 2*b* and *c*) were obtained using a JEOL JSM-6360 scanning electron microscope (accelerating voltage of 15 kV) at the Centre for Instrumental Analysis, Yamaguchi University. The Kreimbach/Kaulbach specimen was analysed using a Zeiss Evo 50 scanning electron microscope (accelerating

https://doi.org/10.1180/minmag.2017.081.020 Published online by Cambridge University Press

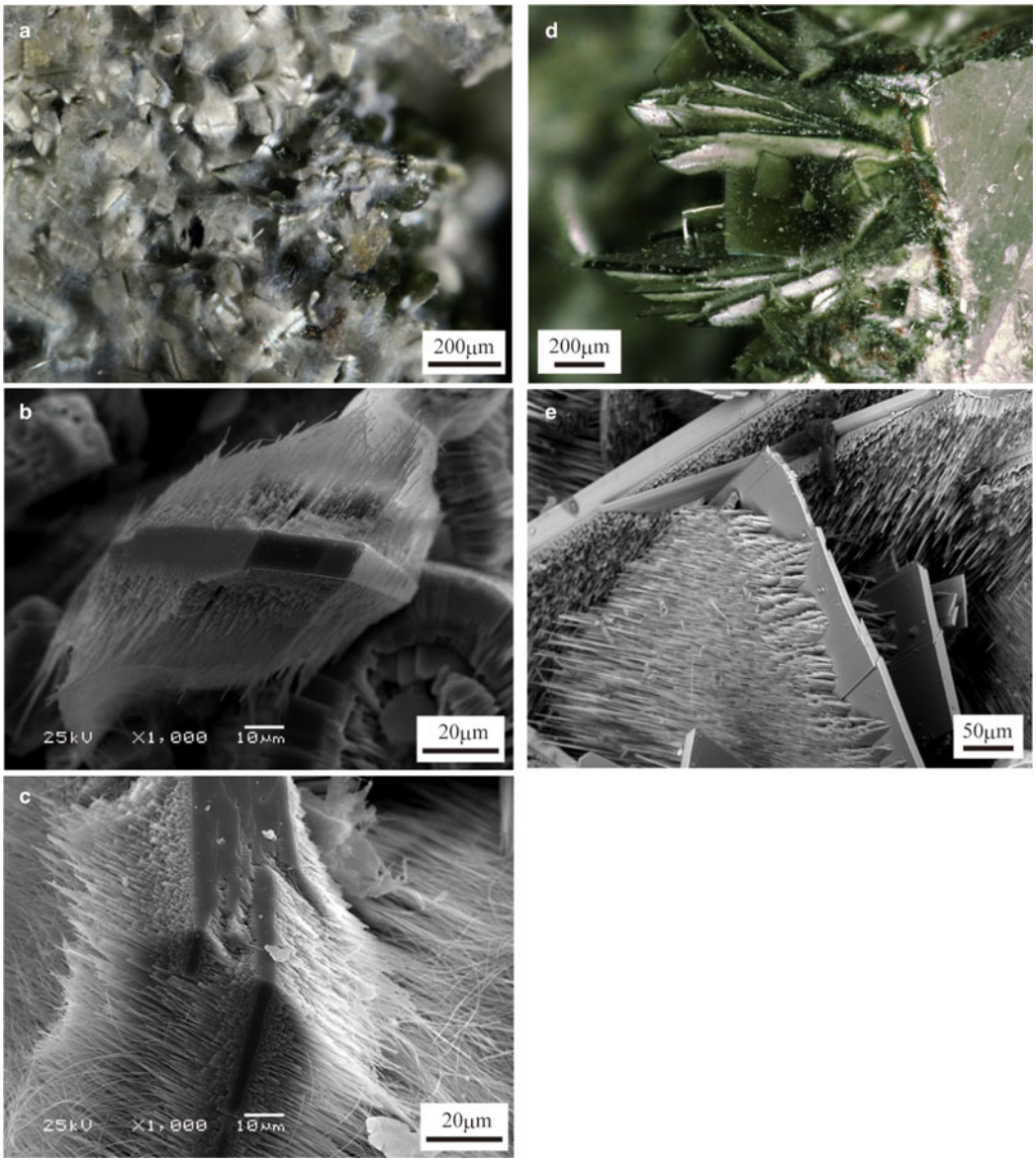

FIG. 1. Photomicrographs (*a*, *d*) and scanning electron images (*b*, *c*, *e*) of babingtonite plates with hedenbergite whiskers from Arvigo (*a*–*c*) and Kreimbach/Kaulbach (*d*, *e*).

voltage of 20 kV) housed at the University of Bern (Fig. 2*e*).

Electron microprobe analysis

The chemical compositions of the babingtonite and the hedenbergite whiskers were determined using the JEOL JXA-8230 electron microprobe analyser (EMPA) at the Centre for Instrumental Analysis, Yamaguchi University. Silicon, Ti, Al, Cr, V, Fe, Mn, Mg, Ca, Sr, Ba, Na, K, Ni, Cu, Zn, Pb, P, F and Cl were measured using an accelerating voltage of 15 kV, a beam current of 20 nA and a beam diameter of 1 μm. The following standards were used: natural wollastonite (Si and Ca), synthetic $KTiPO_4$ (P and K), synthetic $Ca_3(VO_4)_2$ (V),

https://doi.org/10.1180/minmag.2017.081.020 Published online by Cambridge University Press

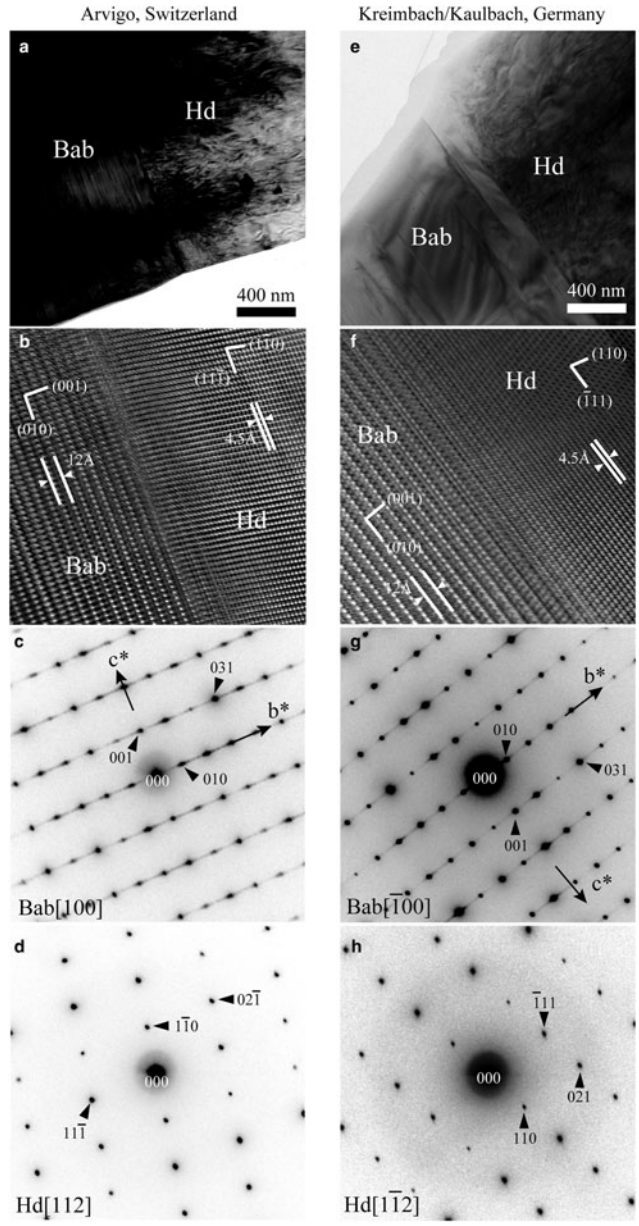

FIG. 2. Transmission electron microscopic (TEM) images of babingtonite and whiskers of hedenbergite at their junctions for Arvigo (*a*–*d*) and Kreimbach/Kaulbach (*e*–*h*) specimens. TEM images (*a* and *e*), HRTEM images (*b* and *f*) and SAED patterns (*c*, *d*, *g* and *h*) are presented for each specimen. The Arvigo specimen was observed along babingtonite [100], and the Kreimbach/Kaulbach sample along babingtonite [$\bar{1}$00].

synthetic rutile (Ti), synthetic corundum (Al), synthetic eskolaite (Cr), synthetic hematite (Fe), synthetic tephroite (Mn), synthetic periclase (Mg), synthetic bunsenite (Ni), PbVGe-oxide (Pb), $SrBaNb_4O_{12}$ (Sr and Ba), albite (Na), orthoclase (K), native copper (Cu), zinc oxide (Zn), synthetic fluorite (F) and synthetic halite (Cl). The elements not listed in Table 1 occurred at concentrations

https://doi.org/10.1180/minmag.2017.081.020 Published online by Cambridge University Press

below the detection limit. The *ZAF* method was used for data correction.

Transmission electron microscope observations

The babingtonite and the hedenbergite whiskers were investigated using transmission electron microscopy with a JEOL JEM-2010 F instrument operated at 200 kV at the Institute for Solid State Physics, University of Tokyo. Specimens for TEM observation were prepared by a JEOL Ion-Slicer. A holder that allows a specimen tilt angle of ±30° was used for TEM observation. Selected area electron diffraction (SAED) patterns were obtained using an aperture of 10 μm diameter, being ~125 nm in real space. We used an objective aperture of 40 μm diameter for high-resolution transmission electron microscopic (HRTEM) images, produced by the interference between transmitted and diffracted waves in the 2θ region above 1.9 Å.

Results

Chemical compositions of the babingtonite and the hedenbergite whiskers

The average compositions of the babingtonite and the whiskers of hedenbergite are given in Table 1. The average chemical composition of Arvigo babingtonite is $(Ca_{2.00}Na_{0.01})_{\sum 2.01}(Fe_{1.45}Mg_{0.28}Mn^{2+}_{0.20}Al_{0.06})_{\sum 1.99}Si_{5.00}O_{14}(OH)$ (number of analytical points, $n = 14$), which lies within the compositional range of the data given by Armbruster (2000). Arvigo babingtonite is characterized by higher contents of Mg (0.28 atoms per formula unit (apfu)) and Mn^{2+} (0.20 apfu) than the Kreimbach/Kaulbach babingtonite (0.15 Mg apfu and 0.08 Mn^{2+} apfu). Total Fe_2O_3 in the Arvigo babingtonite ranges from 19.3 to 22.0 wt.% (1.38–1.56 apfu). Although the quality of compositional data obtained for the hedenbergite (Table 1) is poor due to its fibrous morphology, the composition of hedenbergite whiskers can be represented approximately as $CaFe_{0.5}Mg_{0.5}Si_2O_6$, which corresponds to $Hd_{50}Di_{50}$ in end-member components. The chemical formula of babingtonite from Kreimbach/Kaulbach, derived from the average chemical composition, is $(Ca_{2.01}Na_{0.02})_{\sum 2.03}(Fe_{1.71}Mg_{0.15}Mn^{2+}_{0.08}Al_{0.03})_{\sum 1.97}Si_{5.00}O_{14}(OH)$ ($n = 10$), which is similar to that reported by Bungert *et al.* (1992). The maximum Fe content reached 1.86 Fe apfu, corresponding to 26.02 wt.% total Fe_2O_3. The average end-member composition of the hedenbergite whiskers is $Hd_{58}Di_{31}Ae_{11}$.

The oxidation state of Fe in the babingtonite containing both Fe^{2+} and Fe^{3+} could not be determined because the sample was too small for quantitative ^{57}Fe Mössbauer spectral analysis. The Fe^{2+}/total Fe values, which were calculated based on 29 positive charges to maintain charge balance, were 0.34 for the Arvigo babingtonite and 0.42 for the Kreimbach/Kaulbach babingtonite, corresponding to 1.45 Fe apfu = 0.50 Fe^{2+} + 0.95 Fe^{3+}, and 1.71 Fe apfu = 0.72 Fe^{2+} + 0.99 Fe^{3+}, respectively.

TEM observations

Figure 2 shows TEM images of babingtonite and whiskers of hedenbergite at their junctions for the Arvigo (Fig. 2*a–d*) and Kreimbach/Kaulbach (Fig. 2*e–h*) specimens. Images from TEM (Fig. 2*a* and *e*), HRTEM (Fig. 2*b* and *f*) and SAED patterns (Fig. 2*c*, *d*, *g* and *h*) were obtained for each sample.

In the Arvigo specimen, the boundary between babingtonite and hedenbergite is sharply defined (Fig. 2*a*). Moreover, the HRTEM image clearly shows that both minerals are in direct contact with each other, with no other phases present (Fig. 2*b*). Such a feature suggests some topological relationship between the two minerals. The relationship of babingtonite (Bab) and hedenbergite (Hd) in the Arvigo specimen is Bab[100]//Hd[112], as revealed by the SAED patterns (Fig. 2*c* and *d*). The diffuse streaks along **b*** observed in the electron diffraction pattern of babingtonite (Fig. 2*c*) are caused by chain-periodicity faults (e.g. Czank, 1981). The crystal structure of babingtonite projected along Bab[100] and the structure of hedenbergite projected along Hd[112] is shown in Fig. 3. In the structure along Bab[100], SiO_4 tetrahedra connect with each other via corner sharing, forming chains along the *b* axis. These lead to chain stacking along [001] (Fig. 3*b*). There are two crystallographically non-equivalent octahedrally coordinated sites, M1 and M2, which form clusters of four edge-shared octahedra (Fig. 3*c*). In hedenbergite, SiO_4 tetrahedra are also corner-linked to chains running along the *c* axis (Fig. 3*b*). The Fe-centred octahedra in the hedenbergite structure are also edge-connected and form an octahedral-chain running along the *c* axis (Fig. 3*c*). In the view along Hd[112], the arrangement and the contexture of the SiO_4-chain unit meets with those of babingtonite on Bab[100] (Fig. 3*b*). The *d* spacing and direction of Bab(031)

https://doi.org/10.1180/minmag.2017.081.020 Published online by Cambridge University Press

TABLE 1. Chemical compositions of babingtonite and clinopyroxene.

Locality	Arvigo, Val Calanca, Grisons, Switzerland (NMBE34974)			Kreimbach/Kaulbach, Kaiserslantern, Germany			
	Babingtonite		Whiskered pyroxene*	Babingtonite		Whiskered pyroxene	
	Ave.	Std.		Ave.	Std.	Ave.	Std.
	$n = 14$			$n = 10$		$n = 6$	
SiO_2	53.32	0.33	50.25	52.58	0.28	50.15	0.39
TiO_2	0.01	0.01	0.01	0.01	0.01	0.01	0.01
Al_2O_3	0.51	0.37	0.67	0.30	0.15	0.23	0.07
Cr_2O_3**	0.02	0.03	0.00	0.02	0.03	0.00	0.01
V_2O_3**	0.03	0.02	0.02	0.01	0.02	0.02	0.03
Fe_2O_3**	20.57	0.62		23.94	1.43		
FeO			15.05			20.17	0.86
MnO**	2.47	0.28	1.80	0.95	0.46	1.09	0.40
MgO	1.99	0.28	8.21	1.05	0.46	5.09	0.60
CaO	19.88	0.11	21.80	19.72	0.18	20.83	0.63
BaO	0.03	0.03	0.00	0.02	0.03	0.04	0.04
Na_2O	0.06	0.02	0.36	0.10	0.04	1.43	0.43
K_2O	0.01	0.01	0.02	0.00	0.00	0.00	0.00
NiO	0.01	0.01	0.00	0.02	0.02	0.01	0.02
ZnO	0.03	0.03	0.00	0.03	0.04	0.02	0.02
Total	98.98		98.18	98.76		99.10	
	ΣCations = 9		ΣCations = 4	ΣCations = 9		ΣCations = 4	
Si	5.00	0.01	1.98	5.00	0.01	1.99	0.00
Ti	0.00	0.00	0.00	0.00	0.00	0.00	0.00
Al	0.06	0.04	0.03	0.03	0.02	0.01	0.00
Cr^{3+}	0.00	0.00	0.00	0.00	0.00	0.00	0.00
V^{3+}	0.00	0.00	0.00	0.00	0.00	0.00	0.00
Fe	1.45	0.04	0.50	1.71	0.10	0.67	0.03
Mn^{2+}	0.20	0.03	0.06	0.08	0.03	0.04	0.01
Mg	0.28	0.04	0.48	0.15	0.06	0.30	0.03
Ca	2.00	0.01	0.92	2.01	0.02	0.88	0.03
Ba	0.00	0.00	0.00	0.00	0.00	0.00	0.00
Na	0.01	0.00	0.03	0.02	0.01	0.11	0.03
K	0.00	0.00	0.00	0.00	0.00	0.00	0.00
Ni	0.00	0.00	0.00	0.00	0.00	0.00	0.00
Zn	0.00	0.00	0.00	0.00	0.00	0.00	0.00
Total	9.00		4.00	9.00		4.00	
Constituent end member components of pyroxene							
Diopside (Di: $CaMgSi_2O_6$)			49.3			31.0	
Hedenbergite (Hd: $CaFe^{2+}Si_2O_6$)			47.9			57.6	
Aegirine (Ae: $NaFe^{3+}Si_2O_6$)			2.8			11.4	

*Data quality for clinopyroxene is poor due to its fibrous morphology.
**Total Cr as Cr_2O_3, V as V_2O_3, Mn as MnO, and Fe as Fe_2O_3 in babingtonite, and as FeO in clinopyroxene.

are almost consistent with those of Hd(02$\bar{1}$) (Fig. 3*b*). Indeed, as shown in Fig. 2*c* and *d*, Bab (031) and Hd(02$\bar{1}$) in SAEDs are observed at identical positions. Although the continuity of octahedra between the minerals is different in both structures, the constitution of the cluster composed of four octahedra in the babingtonite structure is consistent with the fragment of four

https://doi.org/10.1180/minmag.2017.081.020 Published online by Cambridge University Press

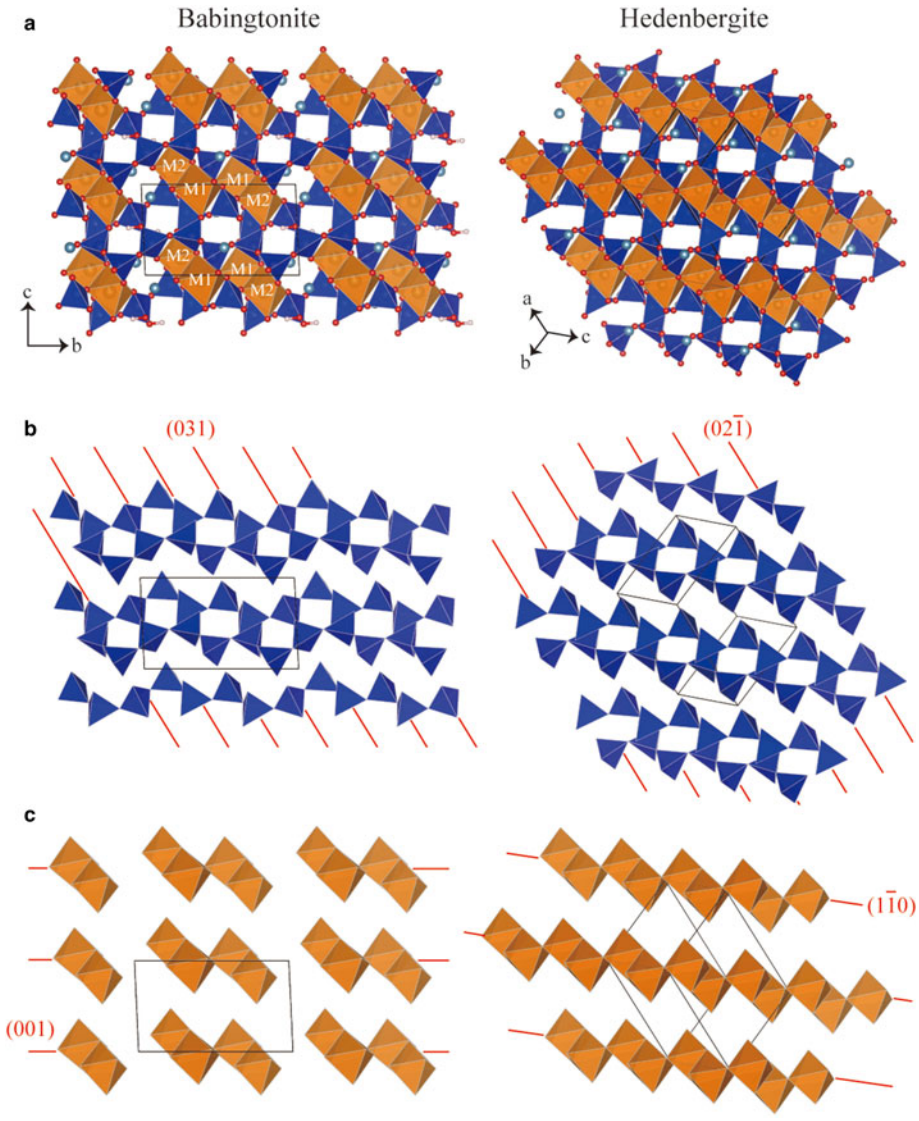

FIG. 3. Crystal structures of babingtonite and hedenbergite (*a*) drawn with the orientation determined using TEM observations of the Arvigo specimen. The crystal structure of babingtonite was projected along [100] and that of hedenbergite along [112]. The arrangements of SiO_4-chain units (*b*) and octahedra (*c*) are shown, drawn using the software *VESTA3* (Momma and Izumi, 2011).

octahedra in the hedenbergite structure (Fig. 3*c*). Thus, the topological relationship can be explained by the arrangements of the SiO_4-chain units and the clusters of octahedra.

The same structural relationship is also observed in the Kreimbach/Kaulbach specimen. The babingtonite and hedenbergite are in direct contact (Fig. 2*f*), and the boundary is sharp. The diffuse streaks along **b*** were also observed in this specimen (Fig. 2*g*), but they tend to be weaker than those observed for the Arvigo babingtonite. The relationship of the babingtonite to the hedenbergite in the Kreimbach/Kaulbach specimen is Bab[$\bar{1}$00]//Hd[1$\bar{1}$2] (Fig. 2*g* and *h*). This direction corresponds to the reverse side of that observed in the Arvigo specimen, and analogously, diffractions

https://doi.org/10.1180/minmag.2017.081.020 Published online by Cambridge University Press

derived from Bab(031) and Hd(021) appear in identical positions. Therefore, the structural relationships of the SiO_4-chain units and the octahedral arrangements in the Kreimbach/Kaulbach material correspond to those defined for the Arvigo sample.

Discussion

Factors controlling coherent growth between pyroxenoid and clinopyroxene

Due to the close orientation relationship of the SiO_4-tetrahedral chains and the configuration of octahedra (Fig. 3), the hedenbergite fibres grew on {010} of the babingtonite (e.g. Armbruster *et al.* 2000, 2002, this study). As shown in Fig. 4, the crystal structure projected onto Hd[100] gives us a direct understanding of this relationship. The reciprocity between babingtonite and hedenbergite is governed by the direction of the SiO_4-tetrahedral chains. The five-periodic tetrahedral chain of babingtonite abruptly changes into the two-periodic chain of hedenbergite. The calculated angle between the chain extension direction of the clinopyroxene and babingtonite (Takéuchi and Koto, 1977) is 16.1°. The octahedral cluster consisting of four octahedra of babingtonite transforms coherently to the octahedral ribbon in hedenbergite. As shown in Fig. 4, the distance between ribbons consisting of the edge-sharing octahedra across a SiO_4-chain in babingtonite and hedenbergite is largely consistent. This distance is ~8.8 Å in the babingtonite structure and ~8.9 Å in hedenbergite, corresponding to the length of the *b* axis.

High-resolution TEM observations of intergrowths of synthetic augite and Fe-rich pyroxenoids (Ried, 1984), and of natural johannsenite and Mn-rich pyroxenoids (Veblen, 1985) indicate that the periodicity faults in clinopyroxene occur parallel to $\{11\bar{1}\}$ (Ried, 1984; Veblen, 1985; Angel, 1986), and this is consistent with our results (Fig. 2*b* and *f*). The orientation relationship between clinopyroxene and pyroxenoid is governed by the same principles in both epitaxial growth and topotaxial intergrowth. Angel (1986) emphasized the importance of the relative positioning of corresponding silicate chains for the transformation between clinopyroxene and bustamite. Because bustamite has silicate chains that are laterally displaced compared with other pyroxenoids, transformation in the solid state between bustamite and either clinopyroxene or pyroxenoid proceeds by a two-step mechanism via an intermediate wollastonite-like structure in order to exceed a low energy activation barrier (Angel, 1986). A continuous change between clinopyroxene and pyroxenoid, with no clearly defined boundary, has also been suggested by Ried (1984), who investigated the indefinite boundary of intergrowths between pyroxferroite and augite (see fig. 1 in Ried, 1984) and proposed that the structures change continuously from one to the other.

The reaction from johannsenite to rhodonite was described by Livi and Veblen (1992), and they observed a metastable mixture of rhodonite and pyroxmangite with high Ca concentrations as an intermediate product. The Ca contents of this mixture (0.4–0.5 Ca apfu normalized as O = 6) exceed the solubility limit of Ca ions in natural rhodonite (~0.2 apfu: e.g. Nelson and Griffin, 2005) and pyroxmangite (~0.1 apfu: Narita *et al.*, 1977; Pinckney and Burnham, 1988). Thus, the intermediate phase plays the role of a compositional buffer zone in a solid-state reaction. A compositional intermediate phase was also suspected in the oriented intergrowth of two other pyroxenoids. Raade and Erambert (1999) reported an intergrowth between scandiobabingtonite, $Ca_2(Fe^{2+}, Mn^{2+})(Sc,Fe^{3+})[Si_5O_{14}(OH)]$ and cascandite, $CaSc[Si_3O_8(OH)]$, from a granite pegmatite in Norway. The authors suggested that the oriented intergrowth was favoured by chain periodicity faults in babingtonite (Czank, 1981). The compositions of the intermediate phases between the two intergrown minerals were interpreted to be the result of structural intermediate states (Raade and Erambert, 1999).

An example of suspected epitaxial growth between chain silicates was addressed by Brugger *et al.* (2006). Saneroite, $Na_{1-1.5}Mn_5[Si_5O_{14}(OH)](Si,V,As)O_3(OH)$ and scheuchzerite, $Na(Mn,Mg)_9[VSi_9O_{28}(OH)](OH)_3$, are both triclinic minerals that have branched silicate chain structures: 5-periodic chains in saneroite and 7-periodic chains in scheuchzerite. In fact, the saneroite chain may be considered a fragment of the more complex scheuchzerite chain. Octahedra in the structures of both these minerals form ribbons, but with different topologies (Brugger *et al.*, 2006). A scanning electron image (fig. 1 in Brugger *et al.*, 2006) shows acicular but flattened scheuchzerite crystals emerging along parallel lines out of a saneroite plate, strongly resembling the epitaxial growth of hedenbergite on babingtonite (fig. 1 in Armbruster *et al.*, 2002). The orientational relationship between the scheuchzerite and saneroite was not investigated, but Brugger *et al.* (2006) convincingly

https://doi.org/10.1180/minmag.2017.081.020 Published online by Cambridge University Press

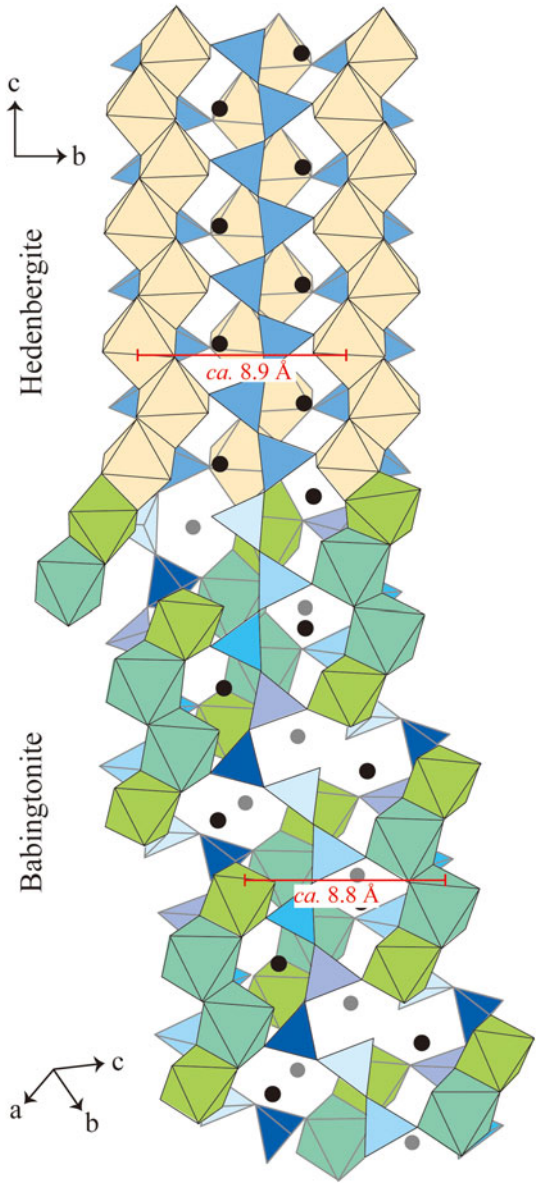

FIG. 4. Polyhedral drawing representing the epitaxial relationship between babingtonite and hedenbergite and showing the tetrahedral chain configuration projected onto hedenbergite [100]. Black circles represent the positions of Ca atoms.

argued that the strong structural and chemical similarities of the two minerals suggest epitaxial growth with a coherent continuation of the silicate chains.

Oriented intergrowths of clinopyroxene and pyroxenoid were interpreted by Ried (1984) to be due to the similar orientations of both the cation octahedra and silicate chains in the corresponding structures. The topology of the octahedra in clinopyroxene and babingtonite are not identical, though their configurations are similar (Fig. 3*c*). There is only one crystallographically independent octahedron in clinopyroxene but two (M1 > M2) in babingtonite. In clinopyroxenes, octahedra form edge-sharing ribbons, whereas the four edge-sharing octahedra (M2–M1–M1–M2) form a cluster in babingtonite (Fig. 3*a* and *c*). Octahedral sites in Hd–Di clinopyroxene are occupied by Fe^{2+} and Mg, but M1 and M2 octahedra in babingtonite are occupied by Fe^{2+} and Fe^{3+}, respectively. Such different cation distributions also affect the volume of the octahedra. However, the different topologies and individual octahedral sizes do not disturb the coherent growth of clinopyroxene on babingtonite. Thus, in general, the similar orientations and placings of SiO_4-chains is the most effective factor in topotaxial transformations and epitaxial growth.

Reports on topotactic intergrowths of chain silicates with different chain periodicities and related topologies of octahedral blocks or ribbons are reasonably common. The vast majority of such intergrowths are due to diffusion-controlled solid-state reactions. Only a few studies have covered the epitaxial growth of different chain-silicate minerals. Such epitaxial pairs are commonly found in vugs or fissures in rocks where the host mineral is primary and the epitaxial guest formed at a later stage under different conditions with regard to fluid composition, temperature and pressure. For rapid whisker growth, supercritical hydrothermal fluids (Bradley *et al.*, 1983), supersaturated solutions or a vapour medium are generally assumed (e.g. Bonev *et al.*, 1985). Thus, epitaxial pairs may crystallize under conditions far from equilibrium, whereas in solid-state reactions diffusion moves the system towards a state of equilibrium. For epitaxial pairs a close chemical relationship between host and guest is not a requirement, but it may favour the coherent growth of different related structures. The key to epitaxial coherence is a strong surface relationship between the contact planes of the host and guest phase. The similarities enable crystallization of the guest phase without supplying the complete nucleation energy. This allows a snapshot in the development of a vug or fissure system because the epitaxial phase commonly only exists due to its nucleation-energy-free crystallization. In the case

https://doi.org/10.1180/minmag.2017.081.020 Published online by Cambridge University Press

of chain silicates, the location of spots on the host and guest surface structures out of which the silicate chains emerge should be preferably 'identical'. This ideal two-dimensional identity is most likely to be achieved in the case of strong structural and chemical similarities. Epitaxial growth of hedenbergite whiskers on a base of {010} plates of babingtonite is marked by an abrupt, but coherent, change of structure at the interface, and represents an almost ideal example where the similar chemical compositions of host and guest strongly contribute to the close structural relationship.

Acknowledgements

Prof T. Armbruster is thanked for supplying us with the Kreimbach/Kaulbach specimen that he received for study from Prof W. Hofmeister, and also for his critical comments on this manuscript. We also thank Dr B. Hoffmann at the Natural History Museum of Bern, for supplying us with the Arvigo babingtonite specimen (Sample No. NMBE34974), Prof M. Akasaka for his critical reading of the first draft, Mr V. Malogajski for his technical assistance in taking the optical photographs, and Dr F. Gfeller and Mr Y. Morifuku for their technical assistance in using the SEM. The Principal Editor Prof P. Williams, as well as Prof G. Ferraris and an anonymous reviewer are thanked for their constructive comments. The TEM session was performed at facilities of the Institute for Solid State Physics, University of Tokyo (project No. BG51, AG78).

References

Akasaka, M., Kimura, T. and Nagashima, M. (2013) Rietveld and ^{57}Fe Mössbauer study of babingtonite from Shimane Peninsula, Japan. *Journal of Mineralogical and Petrological Sciences*, **108**, 121–130.

Angel, R.J. (1986) Transformation mechanisms between single-chain silicates. *American Mineralogist*, **71**, 1441–1454.

Araki, T. and Zoltai, T. (1972) Crystal structure of babingtonite. *Zeitschrift für Kristallographie*, **135**, 355–375.

Armbruster, T. (2000) Cation distribution in Mg, Mn-bearing babingtonite from Arvigo, Val Calanca, Grisons, Switzerland. *Schweizerische Mineralogische und Petrographische Mitteilungen*, **80**, 279–284.

Armbruster, T., Stalder, H.A. and Gnos, E. (2000) Epitaxy of hedenbergite whiskers on babingtonite in Apline fissures at Arvigo, Val Calanca, Grisons, Switzerland. *Schweizerische Mineralogische und Petrographische Mitteilungen*, **80**, 285–290.

Armbruster, T., Gnos, E. and Richards, R.P. (2002) Epitactic hedenbergite whiskers on babingtonite, a second occurrence from a Triassic basalt at Lincoln Park near Paterson, New Jersey, USA. *Schweizerische Mineralogische und Petrographische Mitteilungen*, **82**, 25–32.

Birch, W.D. (1983) Babingtonite, fluorapophyllite and sphene from Harcourt, Victoria, Australia. *Mineralogical Magazine*, **43**, 377–380.

Bonev, I.K., Reiche, M. and Marinov, M. (1985) Morphology, perfection and growth of natural pyrite whiskers and thin platelets. *Physics and Chemistry of Minerals*, **12**, 223–232.

Bradley, J.P., Brownlee, D.E. and Veblen, D.R. (1983) Pyroxene whiskers and platelets in interplanetary dust: evidence of vapour phase growth. *Nature*, **301**, 473–477.

Brugger, J., Krivovichev, S., Meisser, M., Ansermet, S. and Armbruster, T. (2006) Scheuchzerite, Na(Mn, Mg)$_9$[VSi$_9$O$_{28}$(OH)](OH)$_3$, a new single-chain silicate. *American Mineralogist*, **91**, 937–943.

Bungert, R., Konrad, J. and Hofmeister, W. (1992) Babingtonit, $Ca_2Fe^{2+}Fe^{3+}[Si_5O_{14}OH]$, ein Neufund aus den hydrothermalen Alterationszonen der Saar-Nahe-Vulkanite. *Aufschluss*, **43**, 297–299 [in German].

Burns, G.R. and Dyar, M.D. (1991) Crystal chemistry and Mössbauer spectra of babingtonite. *American Mineralogist*, **76**, 892–899.

Burt, D.M. (1971) Multisystems analysis of the relative stabilities of babingtonite and ilvaite. *Carnegie Institute Annual Report Geophysical Laboratory*, **70**, 189–197.

Cameron, M., Sueno, S., Prewitt, C.T. and Papike, J.J. (1973) High-temperature crystal chemistry of acmite, diopside, hedenbergite, jadeite, spodumene, and ureyite. *American Mineralogist*, **58**, 594–618.

Czank, M. (1981) Chain periodicity faults in babingtonite, $Ca_2Fe^{2+}Fe^{3+}H[Si_5O_{15}]$. *Acta Crystallographica,* **A37**, 617–620.

Gole, M.J. (1981) Ca–Fe–Si skarns containing babingtonite: First known occurrence in Australia. *Canadian Mineralogist*, **19**, 269–277.

Graeser, S. and Stadler, H.A. (1976) Mineral-Neufunde aus der Schweiz und angrenzenden Gebieten II. *Schweizer Strahler*, **4**, 158–171 [in German].

Heidtke, U. (1986) Minerale eines Kluftsystems im Steinbruch von Kreimbach (Pfalz). *Aufschluss*, **37**, 395–405 [in German].

Hofmeister, W. and von Platen, H. (1990) Hydrothermale Mineralisationen in subvulkanischen basischen Lagergängen des Saar-Nahe-Gebietes. *Mitteilungen der Pollichia*, **77**, 147–153 [in German].

Liebau, F. (1985) *Structural Chemistry of Silicates: Structure, Bonding, and Classification*, Springer-Verlag, Berlin – Heidelberg.

https://doi.org/10.1180/minmag.2017.081.020 Published online by Cambridge University Press

Livi, K.J. and Veblen, D.R. (1992) An analytical electron microscopy study of pyroxene–pyroxenoids reactions. *American Mineralogist*, **7**, 380–390.

Momma, K. and Izumi, F. (2011) VESTA3 for three-dimensional visualization of crystal, volumetric and morphology data. *Journal of Applied Crystallography*, **44**, 1272–1276.

Nagashima, M., Mitani, K. and Akasaka, M. (2014) Structural variation of babingtonite depending on cation distribution at the octahedral sites. *Mineralogy and Petrology*, **108**, 287–301.

Narita, H., Koto, K. and Morimoto, N. (1977) The crystal structures of $MnSiO_3$ polymorphs (rhodonite- and pyroxemangite-type). *Mineralogical Journal*, **8**, 329–342.

Nelson, W.R. and Griffin, D.T. (2005) Crystal chemistry of Zn-rich rhodonite ("fowlerite"). *American Mineralogist*, **90**, 969–983.

Nolan, J. (1969) Physical properties of synthetic and natural pyroxenes in the system diopside–hedenbergite–acmite. *Mineralogical Magazine*, **37**, 216–229.

Pinckney, L.R. and Burnham, C.W. (1988) Effects of compositional variation on the crystal structures of pyroxemangite. *American Mineralogist*, **73**, 798–808.

Raade, G. and Erambert, M. (1999) An intergrowth of scandiobabingtonite and cascandite from the Heftetjern granite pegmatite, Norway. *Neues Jahrbuch für Mineralogie Monatshefte*, **1999**, 545–550.

Ried, H. (1984) Intergrowth of pyroxene and pyroxenoid; chain periodicity faults in pyroxene. *Physics and Chemistry of Minerals*, **10**, 230–235.

Rutstein, M. and Yund, R.A. (1969) Unit-cell parameters of synthetic diopside–hedenbergite solid solutions. *American Mineralogist*, **54**, 238–245.

Takéuchi, Y. and Koto, K. (1977) A systematics of pyroxenoid structures. *Mineralogical Journal*, **8**, 272–285.

Veblen, D.R. (1985) TEM study of a pyroxene-to-pyroxenoid reaction. *American Mineralogist*, **70**, 885–901.

Weisenberger, T. and Bucher, K. (2010) Zeolites in fissures of granites and gneisses of the Central Alps. *Journal of Metamorphic Geology*, **28**, 825–847.

Weisenberger, T. and Bucher, K. (2011) Mass transfer and porosity evolution during low temperature water-rock interaction in gneisses of the simano nappe: Arvigo, Val Calanca, Swiss Alps. *Contributions to Mineralogy and Petrology*, **162**, 61–81.

Wise, W.S. and Moller, W.P. (1990) Occurrence of Ca–Fe silicate minerals with zeolites in basalt cavities at Bombay, India. *European Journal of Mineralogy*, **2**, 875–883.

https://doi.org/10.1180/minmag.2017.081.020 Published online by Cambridge University Press